Pergamon

Ultrasound in Med. & Biol., Vol. 21, No. 5, pp. 657–670, 1995

0301-5629/95 $9.50 + .00

0301-5629(94)00156-1

●*Original Contribution*

THE BUTTERFLY SEARCH TECHNIQUE FOR ESTIMATION OF BLOOD VELOCITY

SHEIKH KAISAR ALAM and KEVIN J. PARKER
Department of Electrical Engineering, University of Rochester, Rochester, NY, USA

(*Received* 3 *June* 1994; *in final form* 15 *November* 1994)

Abstract—We present a novel, robust and accurate blood velocity estimation technique that is implementable by elementary digital signal processing. In this technique, echoes from repeated firings of a transducer are resampled along a set of predetermined trajectories of constant velocities, called "butterfly lines" because of their intersection at a reference range. The slope of the trajectory on which the sampled signals satisfy a predetermined criterion appropriate for the type of signal in question, provides an estimate of the velocity of the target. The search for this trajectory is called "butterfly search," which can be carried out efficiently in a parallel processing scheme. The estimator can be based on the RF echo, its envelope, or its quadrature components. We present the theory of the butterfly search and some preliminary results. The butterfly search on quadrature components has shown superior noise immunity, with relatively few successive scan lines, and was found to outperform all the common time domain and Doppler techniques in simulations and phantom experiments with strong noise. The butterfly search can overcome many disadvantages faced by the present day techniques, such as the stringent tradeoff criterion between imaging resolution and velocity resolution implicit in Doppler techniques, and the need for computation-intensive operations.

Key Words: **Ultrasound, Velocity, Doppler, Pulsed Doppler, Blood flow, Color flow imaging, Color Doppler imaging.**

INTRODUCTION

Real-time transcutaneous blood flow velocity measurement plays a major role in the diagnosis of many vascular diseases, especially cardiac diseases. Pulsed Doppler ultrasound has long been used as the method of choice for this purpose. A reflected ultrasound wave undergoes a Doppler shift in frequency if the reflector moves toward or away from the receiver. The shift f_d can be expressed by:

$$f_d = \frac{2v_0 \cos\theta}{c} f_0 \qquad (1)$$

where f_0 is the frequency of the continuous emitted wave, v_0 is the velocity of the reflector, c is the velocity of the wave in medium and θ is the angle between the direction of movement of the reflector and the direction of the beam. However, the conventional pulsed Doppler and color Doppler machines do not use the Doppler shift for estimating the velocity, since range resolution cannot be obtained with continuous-wave isonation. In the past, several different techniques have been proposed and some have been implemented in clinical pulsed imaging instruments. Among the most common of them, some make use of the change of phase of a reflected signal (Doppler techniques—Angelsen 1981; Kasai et al. 1985; Magnin 1986) while many others make use of the time shift in the envelope or RF signals using correlation methods (time domain techniques—Bonnefous and Pesque 1986; Embree and O'Brien 1990; Foster et al. 1990; Pesque 1989). However, all of them require various tradeoffs. With the Doppler techniques, a relatively long tone burst is needed to accurately measure the velocity. This decreases the flow imaging resolutions. In time domain techniques, correlation windows must be fixed, and extensive calculations over many echo pairs are required. More recently, an important matched filter approach to a maximum likelihood estimator of velocity was developed by Ferrara and Algazi (1991a,b).

Typical values of the signal-to-noise-ratio (SNR) are in the range of 0 to 20 dB, since blood backscatter is weak. So, the estimation techniques must perform well in noisy situations. Computational complexity is another issue in evaluating the merits of an estimation

Address correspondence to: Kevin J. Parker, Ph.D., Department of Electrical Engineering, Hopeman Engineering Building #203, University of Rochester, Rochester, NY 14627, USA.

technique. Finally, the number of successive scan lines required to arrive at a velocity estimate is important since this relates to the color flow imaging rate of an instrument. The method proposed herein combines some of the best features of time domain and Doppler methods. The method is readily realizable in hardware without extensive correlation calculations. It performs well with a wideband pulse in the presence of noise and requires fewer successive lines than many other techniques. The method is described after a brief review of the prior developments. All the techniques are discussed for a moving point scatterer for convenience.

BACKGROUND

Doppler ultrasound

Pulsed Doppler systems transmit a short sinusoidal burst instead of a continuous sinusoid. By gating the received signals to correspond to the pulse's time of flight to the point of interest, one can interrogate a small sample volume instead of the entire length of the beam. It is lucidly described in a tutorial article by Magnin (1986).

Samples of the Doppler signal are obtained by sampling the echo at a fixed range. For the purpose of illustration, let us consider an object moving toward the transducer (for simplicity, a point target is being used for all illustrations). As the object advances, the phase changes corresponding to the distance the target has moved between successive samples. If the velocity v_0 is constant, then the nth RF A-line from a point spread target would have the form

$$s(n, t) = A \cos\left\{\omega_0\left[t - 2\frac{d}{c} + 2n\frac{v_0}{c}T\right]\right\} \times r\left\{t - 2\frac{d}{c} + 2n\frac{v_0}{c}T\right\}$$

$$n = 0, 1, 2, \ldots, N-1. \quad (2a)$$

In discrete time representation

$$s[n, i] = A \cos\left\{\omega_0\left[\frac{i}{f_f} - 2\frac{d}{c} + 2n\frac{v_0}{c}T\right]\right\} r\left\{\frac{i}{f_f} - 2\frac{d}{c} + 2n\frac{v_0}{c}T\right\} \quad (2b)$$

where A is the signal amplitude, n is the index for the repeated echo lines (slow-time index), T is the pulse repetition period, f_f is the fast time sampling frequency, d is the initial distance of the object from the transducer, ω_0 is the angular center frequency, $r(t)$ is the envelope of the transmitted pulse which maximizes at $t = 0$ and the factor of 2 in the expression comes from the round-trip travel of the wave. Time-axis origin is reset each time the transducer fires. System effects are neglected. We will use the terms "slow time, fast time" to refer to samples taken along the (n, t) directions, respectively.

To get the in-phase component $i(n, t)$ and quadrature component $q(n, t)$, $s(n, t)$ should be multiplied by $\cos(\omega_0 t)$ and $\sin(\omega_0 t)$, respectively, and then low-pass filtered.

Then, the complex envelope can be shown to be

$$\tilde{r}(n, t) = i(n, t) + jq(n, t)$$

$$= \frac{A}{2}\exp j\left[2\omega_0\left(\frac{d}{c} - n\frac{v_0}{c}T\right)\right] r\left\{t - 2\frac{d}{c} + 2n\frac{v_0}{c}T\right\}$$

$$= \tilde{A}\exp -j\left[2\omega_0 n\frac{v_0}{c}T\right] \times r\left\{t - 2\frac{d}{c} + 2n\frac{v_0}{c}T\right\},$$

$$\text{where} \quad \tilde{A} = \frac{A}{2}\exp j\left[2\omega_0\frac{d}{c}\right]. \quad (3a)$$

In discrete time representation

$$\tilde{r}[n, i] = \tilde{A}\exp -j\left[2\omega_0 n\frac{v_0}{c}T\right] \times r\left\{\frac{i}{f_f} - 2\frac{d}{c} + 2n\frac{v_0}{c}T\right\}. \quad (3b)$$

If the complex envelope of the reflection is sampled at a constant range (or equivalently, at a constant time $t = t_s$), its peak frequency will be proportional to the velocity, provided that no aliasing has occurred, and $R(\omega)$, the spectrum of $r(t)$, maximizes at $\omega = 0$. The general concept is illustrated in Fig. 1, where a single scatterer is assumed, and the envelope $r(t)$ in the figure is nonzero for three and a half periods, and it remains constant within that interval.

Various spectral estimation techniques, including FFT, can be used to estimate the peak frequency. Mo et al. (1988) presented a detailed discussion on a few maximum frequency estimators for Doppler ultrasound.

To estimate the mean frequency, rate of change of phase of the autocorrelation function taken along the "slow time" axis (shown in Fig. 1) can be used (Kasai et al. 1985)

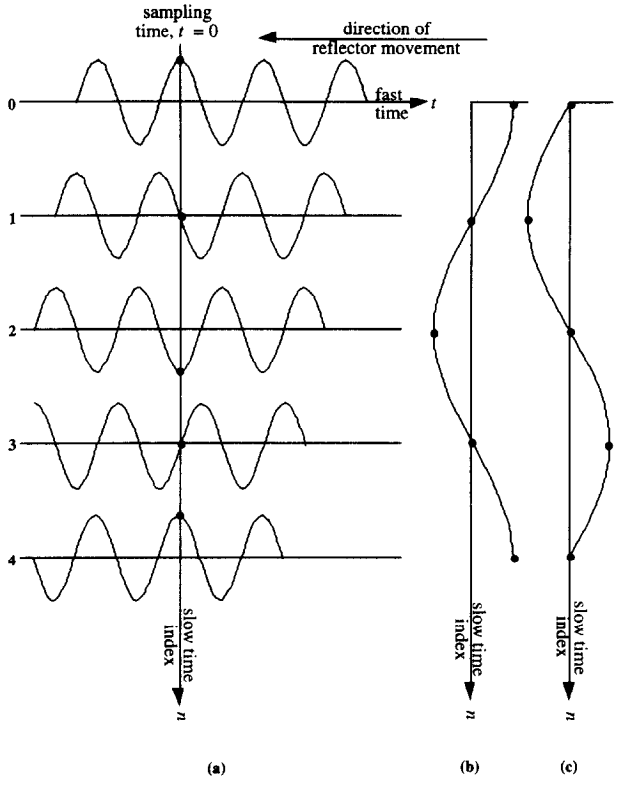

Fig. 1. Illustration of quadrature technique. (a) Reflections and sampling. (b) Sampled signal, and also the in-phase component I. (c) Quadrature component Q.

$$\bar{\omega} = \frac{1}{j}\frac{\dot{R}(0)}{R(0)} = \dot{\phi}(0) \approx \frac{\phi(T)}{T} \tag{4}$$

where $R(\tau)$ is the autocorrelation function of the complex envelope sampled at constant range, and $\phi(\tau)$ is the phase of the autocorrelation function $R(\tau)$, as we can write $R(\tau)$ in the following form

$$R(\tau) = |R(\tau)|\, e^{j\phi(\tau)}. \tag{5}$$

Time domain correlation search

Since a moving scatterer introduces time shift in the reflected ultrasound signal, blood velocity can be found by a straightforward cross-correlation search technique (Bonnefous and Pesque 1986; Embree and O'Brien 1990; Foster et al. 1990).

For variables X and Y consisting of N discrete values, coefficient of correlation ρ_{xy} can be written as

$$\rho_{xy}[i] = \frac{\sum_{k=0}^{N-1} \{x[k] - \bar{X}\}\{y[k+i] - \bar{Y}\}}{\sqrt{\sum_{k=0}^{N-1} \{x[k] - \bar{X}\}^2 \sum_{l=0}^{N-1} \{y[l+i] - \bar{Y}\}^2}}. \tag{6}$$

If X and Y are successive RF A-lines, the maximum of the cross-correlation coefficient ρ_{xy} can be used to estimate the time shift between them caused by scatterer movement, if any, and equivalently, the scatterer velocity. In reality, the true location of the maxima of ρ_{xy} may not be constrained within the integer increments, and will generally lie between the discrete maximum and one of the two neighboring points. An estimate of the true maximum can be obtained by a parabolic interpolation (Foster et al. 1990). To get good results from the correlation techniques in the presence of noise, some temporal averaging may be required.

Bohs and Trahey (1991) proposed to use the sum-absolute-difference (SAD) for flow imaging. It is computationally simpler than the cross-correlation search, but performs nearly as well. The displacement between successive RF A-lines is estimated by finding the minimum of SAD. Sum-absolute-difference for one-dimensional signals is given as

$$\epsilon_{xy}[i] = \sum_{k=0}^{N-1} |x[k] - y[k+i]|. \tag{7}$$

Pesque (1989) proposed using first order Taylor series expansion of the reflections from a moving target to estimate the time shift between successive firings. This method requires the calculation of the first derivative of the signal, and the calculation of derivatives is poorly conditioned in the presence of noise.

Wideband maximum likelihood estimation (WMLE)

This estimator, developed by Ferrara and Algazi (1991a,b), incorporates correlation in the context of a classical matched filter. However, unlike cross-correlation techniques, which use only shift in time, wideband MLE utilizes both the time and frequency shift embodied in a matched filter to estimate velocity. The likelihood function for a point target is given by

$$l(v) = \left| \sum_k \int_{-\infty}^{\infty} r'(t) s'^{*}\left(t - \tau_0 - kT\left[1 + 2\frac{v}{c}\right]\right) \exp(j\sigma v t)\, dt \right|^2 \tag{8}$$

where $s'(\cdot)$ is a delayed version of the complex envelope of the transmitted pulse (including effects of signal propagation and scattering), $r'(t)$ is the complex envelope of the received signal, τ_0 corresponds to the round-trip travel time, and $\sigma = 2\omega_0/c$. In this expression, the time origin is not reset after each transducer firing.

The velocity estimate can be obtained from the

maximum of $l(v)$, or using the following expression that would give the mean velocity

$$\bar{v} = \frac{\sum_i v_i l(v_i)}{\sum_i l(v_i)}. \quad (9)$$

Other methods

The previous sections presented an overview of some widely discussed techniques for blood velocity estimation. There are many excellent review and application articles on both Doppler (Angelsen 1981; Vaitkus and Cobbold 1988; Vaitkus et al. 1988) and time domain methods (Hein and O'Brien 1993).

Some other approaches have been discussed. Barber et al. (1985) proposed a time domain processing scheme of the quadrature components to detect the Doppler frequency. Baek et al. (1989) proposed tracking mean frequencies along the spatial axis with the assumption of continuity of flow to solve the frequency aliasing problem. de Jong et al. (1990) developed an interpolation method which calculates the correlation coefficient only at five points in the vicinity of the maximum, and use an interpolation algorithm to evaluate the location of correlation maximum from these points. This method requires significantly less number of computations compared to correlation search. However, it does not work well with large bandwidth signals, and suffers from aliasing.

Fan and Evans (1994) proposed a Wigner distribution function method that uses a pseudo-instantaneous mean frequency. Wigner distribution function does not require the analyzed signals to be stationary. The instantaneous frequency derived using the Wigner distribution function suffers from spike problems and is quite unstable when the input signal contains more than one frequency component which is usually the case for Doppler signals. The proposed pseudo-instantaneous mean frequency can overcome these problems. Wilson (1991) introduced a broadband pulsed Doppler scheme using 2-D Fourier transform in slow time, fast time. A method to overcome the frequency aliasing problem was also discussed. Sturgill (1990) developed a maximum entropy velocity estimation strategy in which an average power spectrum of the series of received signals is calculated by fitting a polynomial to the series of received echoes. A peak center frequency shift associated with the data for each point is derived from the power spectrum that is used to produce a velocity estimate for that point.

THE BUTTERFLY SEARCH

RF or envelope search—a time domain technique

We propose a simpler technique where a search is performed along trajectories that describe lines of constant velocity in two-dimensional (slow time, fast time) space. In Fig. 2, the envelope of echoes from a single reflector is shown. As the reflector moves, the echoes are time-shifted. Consider a reference sample point at the middle of a few successive A-lines. Then sample at different delays between successive A-lines, or on different trajectories ("butterfly lines" from the shape indicated in Fig. 3). If the delay trajectory matches the scatterer movement, that is, on the butterfly line corresponding to the correct velocity, all the data samples would have the same value and their variance will be zero. To take the presence of noise into account, however, the butterfly lines on which the variance is minimum is searched for. The concept is clearly illustrated in Fig. 3 (where the RF pulse has Gaussian envelope). The solid line is the correct butterfly line, and on it, all the samples have the same value, and hence, zero variance.

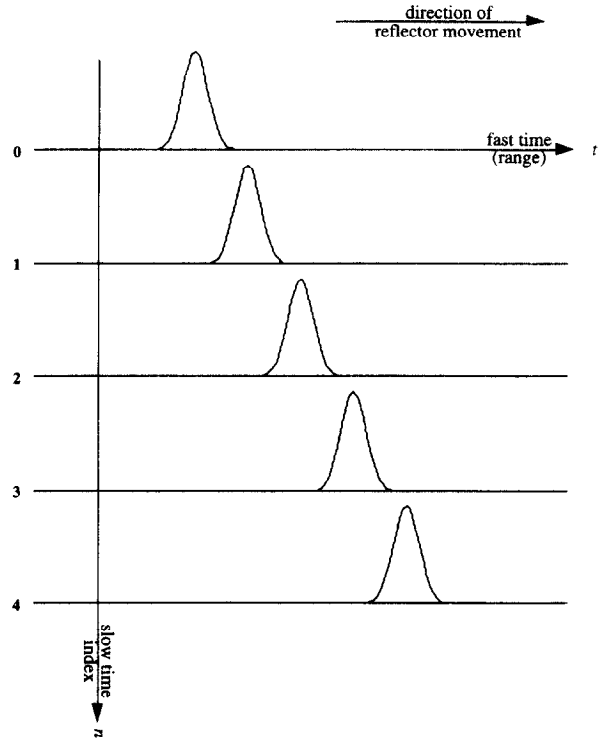

Fig. 2. Illustration of movement of envelope on the time frame with the movement of the scatterer.

Using the same notation as used previously, the envelope $e(n, t)$ for the nth RF A-line

$$e(n, t) = Ar\left\{t - 2\frac{d}{c} + 2n\frac{v_0}{c}T\right\}$$
$$n = 0, 1, 2, \ldots, N-1. \quad (10)$$

To sample $e(n, t)$ at its maximum value over increasing n, the quantity $t - 2\frac{d}{c} + 2n\frac{v_0}{c}T$ should be zero, since $r(\,)$ maximizes at $t = 0$, *i.e.*

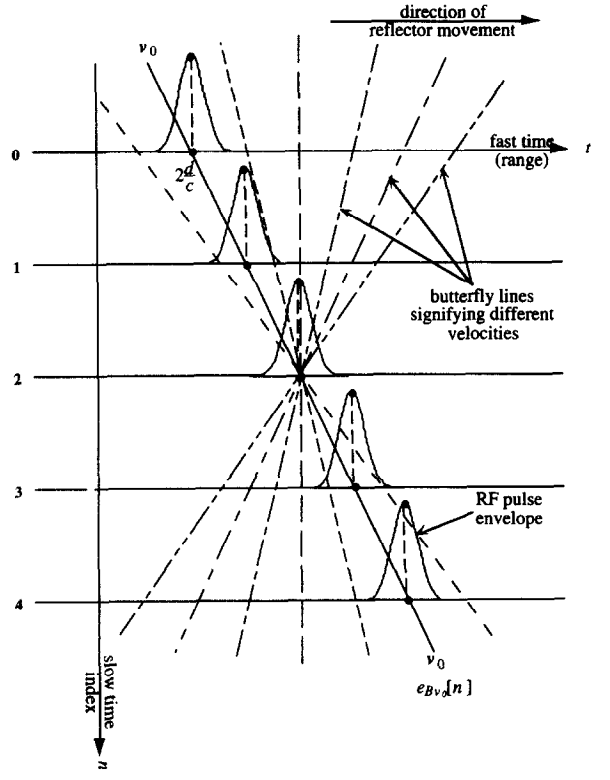

Fig. 3. Illustration of butterfly search (on envelope). Only on the solid line will all the samples have the same value.

$$t - 2\frac{d}{c} + 2n\frac{v_0}{c}T = 0. \tag{11a}$$

In discrete time form

$$\frac{i}{f_f} - 2\frac{d}{c} + 2n\frac{v_0}{c}T = 0. \tag{11b}$$

However, i can have only integer values, and thus, a point on the butterfly line may lie between two successive values of i. Linear interpolation between successive sample points can be used in such cases to estimate the signal value on the butterfly line.

Let us define $e_{Bv}[n]$ to denote the resampling of the envelope along the butterfly line for velocity v to estimate the velocity at depth d

$$e_{Bv}[n] = e(n, t)\delta\left(t - 2\frac{d}{c} + 2n\frac{v}{c}T\right). \tag{12}$$

Here we assume that the impulse train of the sample function is implicitly followed by a conversion to a discrete time sequence (a C/D conversion in the conventional sense) (Oppenheim et al. 1983). Thus

$$e_{Bv_0}[n] = Ar(0). \tag{13}$$

Thus, in the absence of noise, $e_{Bv_0}[n]$ maximizes to a constant value for all n. In other words, the variance of $e_{Bv_0}[n]$ is zero. In the presence of noise, however, this variance is expected not to be zero but a minimum on the correct butterfly line corresponding to v_0. Or, in other words, given the butterfly line with minimum variance, the slope can be used for the scatterer velocity estimation.

The estimated velocity would be found as follows

$$\hat{v} = \min_{v} \{\mathrm{var}(e_{Bv}[n])\} \tag{14}$$

where $\mathrm{var}(e_{Bv}[n])$ is the variance of the envelope sampled on the butterfly line corresponding to velocity v.

We note that the symmetric butterfly centered in slow time (Fig. 3) can be replaced with a "V" or "inverted V" shaped orientation of search lines emanating from the last or the first scan line (Fig. 4).

The same method can be applied to the RF signal. The estimated velocity would then be found as follows

$$\hat{v} = \min_{v} \{\mathrm{var}(s_{Bv}[n])\} \tag{15}$$

where

$$s_{Bv}[n] = s(n, t)\delta\left(t - 2\frac{d}{c} + 2n\frac{v}{c}T\right). \tag{16}$$

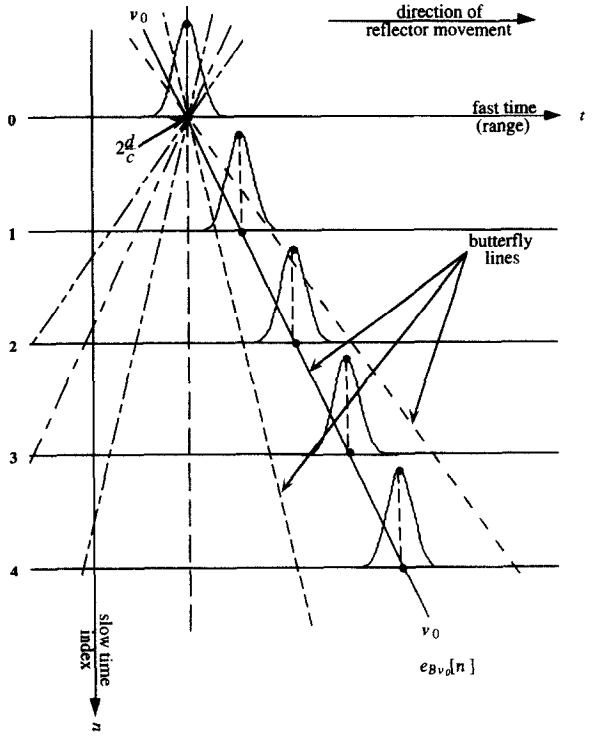

Fig. 4. Alternate butterfly search style ("inverted Vee" search). Only on the solid line will all the samples have the same value.

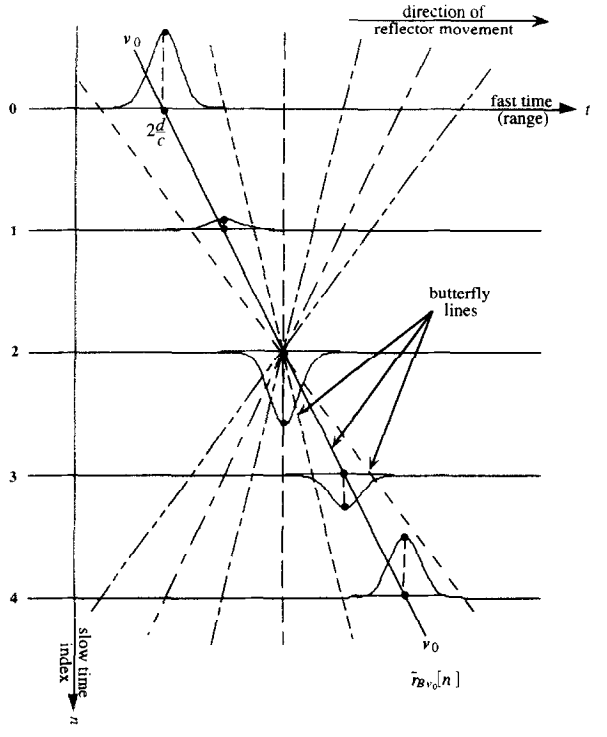

Fig. 5. Illustration of butterfly technique applied on the quadrature components (one shown). Only the solid line would sample a constant amplitude sinusoidal function $\tilde{r}_{Bv_0}[n]$.

Butterfly search on quadrature components—a hybrid technique

The butterfly search on RF and envelope signals are time domain methods. In the butterfly search on quadrature components, the aspects of time domain and frequency domain analyses are combined. The concept is that, for a single target moving at a constant velocity, the quadrature components sampled along the correct butterfly line will be single frequency sinusoids. The frequency of these sinusoids depends on target velocity. So, for each velocity there is a unique correct butterfly line and the complex envelope sampled on that line will have a unique frequency. Thus, we conduct a search where the complex envelope sampled on each butterfly line will be checked for the unique frequency that the sampled complex envelope would have if the target had velocity corresponding to that butterfly line. The method is illustrated in Fig. 5.

From eqn (3a), the complex envelope is

$$\tilde{r}(n, t) = \tilde{A} \exp - j\left[2\omega_0 n \frac{v_0}{c} T\right] \times r\left\{t - 2\frac{d}{c} + 2n \frac{v_0}{c} T\right\}. \quad (17)$$

Following the previous discussions concerning the RF or envelope search, let us define $\tilde{r}_{Bv}[n]$ to denote the resampling of the complex envelope along the butterfly line for velocity v to estimate the velocity at depth d

$$\tilde{r}_{Bv}[n] = \tilde{r}(n, t)\delta\left(t - 2\frac{d}{c} + 2n \frac{v}{c} T\right)$$

$$= \tilde{A} \exp - j\left\{2\omega_0 n \frac{v_0}{c} T\right\} r\left(2n \frac{v_0 - v}{c} T\right). \quad (18)$$

Then, the complex envelope along the correct sampling trajectory is given by

$$\tilde{r}_{Bv_0}[n] = \tilde{A} \exp - j\left[2\omega_0 n \frac{v_0}{c} T\right] r(0). \quad (19)$$

Thus, as also depicted in Fig. 5 (which illustrates the technique as applied for a single point spread target with no noise present), the complex envelope along the *correct butterfly line* would sample a *single frequency* constant amplitude complex exponential with respect to the index n. And, for each velocity, on the correct butterfly line, that distinct frequency is unique. Thus, the signal energy on the correct butterfly line would be concentrated at that frequency. With noise present, that particular frequency would still be expected to have the maximum energy. If we examine each butterfly line for the power contained in the frequency corresponding to that line, normalized by the total power, the maximum should occur on the correct line ($v = v_0$).

To illustrate this, we assume the situation of Fig. 5 and examine samples along other butterfly lines. On an incorrect line, the butterfly sampled complex envelope is given by eqn (18) for $v \neq v_0$. As $\tilde{r}_{Bv}[n]$ varies with n, these signals are now amplitude modulated. Here, the spectrum of $\tilde{r}_{Bv}[n]$ would have the maximum at $\omega = -2\omega_0 \frac{v_0}{c} T$, and not at $\omega = -2\omega_0 \frac{v}{c} T$, although the energy would be spread according to the spectrum of the envelope term $r(\,)$.

We determine the normalized frequency-specific energy along each butterfly line by applying orthogonality and Schwartz's inequality. For each butterfly line the following ratio is evaluated

$$L(v) = \frac{\left|\sum_n \tilde{r}_{Bv}[n] e^{j2\omega_0 n(v/c)T}\right|^2}{\sum_n |\tilde{r}_{Bv}[n]|^2} \quad (20)$$

where $\tilde{r}_{Bv}[n]$ is given by eqn (18) and, $L(v)$ maximizes only at $v = v_0$. The derivation of $L(v)$ is given in the Appendix I.

We estimate the velocity by finding the maximum of $L(v)$,

$$\hat{v} = \max_{v} \{L(v)\} \tag{21}$$

and the mean velocity can be estimated by finding the following weighted mean

$$\bar{v} = \frac{\sum_i \hat{v}_i L(\hat{v}_i)}{\sum_i L(\hat{v}_i)}. \tag{22}$$

Despite the fact that our technique uses quadrature components for the estimation, it does not have the aliasing problem. Although the frequency along a butterfly line can be the same as that on other lines of different velocities due to aliasing, the frequency-specific energies on these incorrect lines are reduced by severe amplitude modulation and interference from the neighboring scatterers. The results in the later sections will demonstrate that the butterfly search on quadrature components does not have the aliasing problem. We note also that a wideband pulse *increases* the discrimination of velocities in the butterfly search. This is in marked contrast to "Doppler" techniques where a short, broadband pulse produces unwanted spectral spreading and other problems. For either envelope, or RF, or complex envelope search, if a finite number of butterfly lines are directly implemented in hardware, there will be a quantization effect in the velocity estimates. However, we can minimize this effect by taking large number of lines. A compromise between quantization error and computational complexity can be made.

HARDWARE IMPLEMENTATION

This technique has an obvious advantage over many of the existing techniques since direct digital implementation is possible without the use of correlations, transforms, iterations or any other complex algorithms. The implementation is quite straightforward. For any signal $r(n, t)$, $r_{Bv}[n]$ is easily sampled as shown in the butterfly sampler in Fig. 6. For envelope processing, envelopes are sampled at the butterfly sampler banks following envelope detection. Each butterfly sampler is connected to a variance detector. The outputs of the variance detectors are fed to a minimum detector. The velocity corresponding to the variance detector producing the minimum, is the estimated velocity. The schematic diagram is shown in Fig. 7.

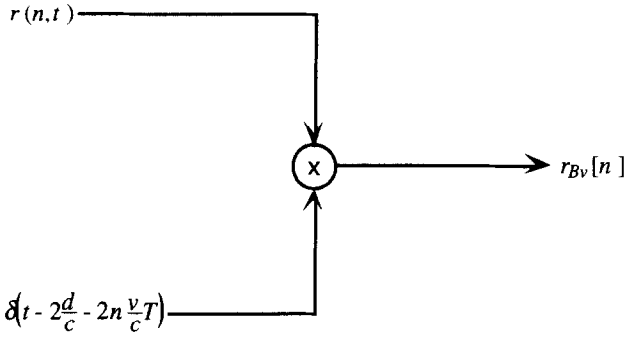

Fig. 6. Butterfly sampler.

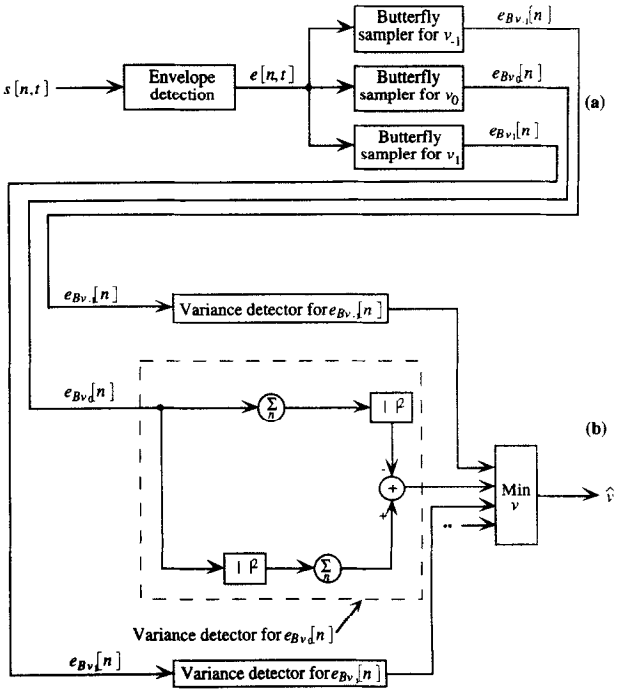

Fig. 7. Schematic hardware diagram for butterfly search on envelope: (a) generating butterfly sampled envelope $e_{Bv}[n]$; (b) processing $e_{Bv}[n]$ to extract $\hat{v}$.

For the RF processing, the schematic hardware is identical to the one shown in Fig. 7, except that the envelope detector is removed.

A block diagram of a possible hardware realization of butterfly search on quadrature components is shown in Fig. 8. Following the quadrature demodulation step, $\tilde{r}_{Bv}[n]$ are sampled at the butterfly sampler banks. The output from each sampler is then fed to a "correspondence detector" involving the following steps: multiplication by an appropriate complex exponential, summation (over index n), followed by magnitude square and a normalization by a quantity that is derived by feeding $\tilde{r}_{Bv}[n]$ through a magnitude square followed by summation (over index n). The $L(v)$ values thus produced are input to a maximum detector. The velocity corresponding to the maximum $L(v)$ is the estimated velocity.

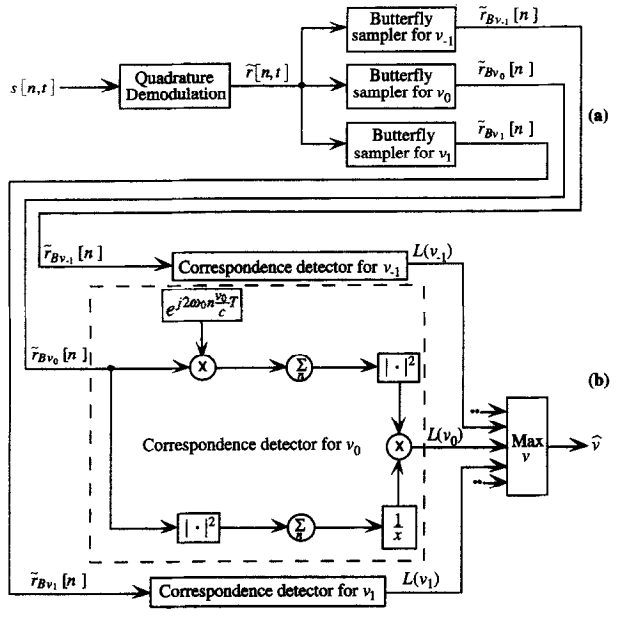

Fig. 8. Schematic hardware diagram for quadrature butterfly search: (a) generating butterfly sampled complex envelope $\tilde{r}_{Bv}[n]$; (b) processing $\tilde{r}_{Bv}[n]$ to extract $\hat{v}$.

SIMULATION METHODS AND RESULTS

Some simulation results for the common time and frequency domain techniques and the proposed technique are given in this section. Results for a single realization of a high noise case are given for quadrature, autocorrelation, cross-correlation, SAD and butterfly techniques with three fast lines. Constant, uniform velocity was used in these simulations. A line of 1024 scatterers was used, which amounted to ~15 mm of tissue.

We used a Gaussian RF pulse, with center frequency $f_0 = 5$ MHz, $\sigma = 1.41$ MHz and $f_s = 50 \times 10^6$/s (PRF = 5 KHz). The pulse is shown in Fig. 9.

The pulse can be expressed in continuous time domain as

$$s(t) = 2\sqrt{2\pi}\sigma e^{-2(\pi\sigma t)^2}\cos(2\pi f_0 t) \qquad (23)$$

from the equivalent frequency domain representation

$$e^{-1/2\sigma^2(f-f_0)^2} + e^{-1/2\sigma^2(f+f_0)^2}. \qquad (24)$$

The 60-dB pulse width for the pulse is $w_{60\,\mathrm{dB}} = \frac{1.18}{\sigma} = 0.84$ μs, which is equivalent to 42 samples, or 0.63 mm of tissue, whereas the 10-dB bandwidth of the pulse is $W_{10\,\mathrm{dB}} = 3.04\sigma = 4.28$ MHz.

The pulse was convolved with a line of random scatterers to produce a fully developed speckle. RF A-lines were quantized at ten bits. One envelope of a scan line is shown in Fig. 10. There was no additive noise.

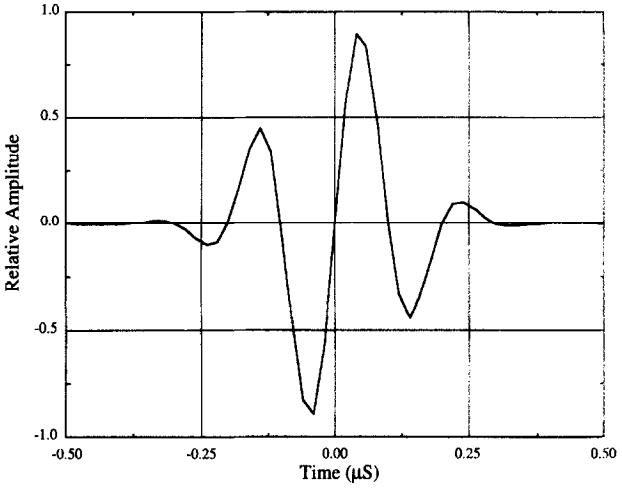

Fig. 9. Pulse fired by the transducer; $\sigma = 1.41$ MHz.

$L(v)$ [eqn (20)] *vs.* v with four RF lines is shown in Fig. 11. The actual scatterer velocity is −75 cm/s, and there was no additive noise. $L(v)$ exhibits a sharp peak at −75 cm/s, as expected. The subsidiary peaks at aliasing interval of 75 cm/s are seen. In general, as the number of RF lines decreases, the peak broadens and the subsidiary peaks increase. Addition of noise brings up the base level.

Graphs of var($s_{Bv}[n]$) *vs.* v (for RF processing) and var($e_{Bv}[n]$) *vs.* v (for envelope processing) for four RF lines are shown in Fig. 12. No additive noise is present, and the actual velocity is −75 cm/s. var($s_{Bv}[n]$) shows a sharp notch (close to zero) at −75 cm/s. var($e_{Bv}[n]$) reaches the minimum at −75 cm/s. In general, the notches broaden as number of RF lines decreases. In general, the addition of noise makes the notch less distinct as a global minimum.

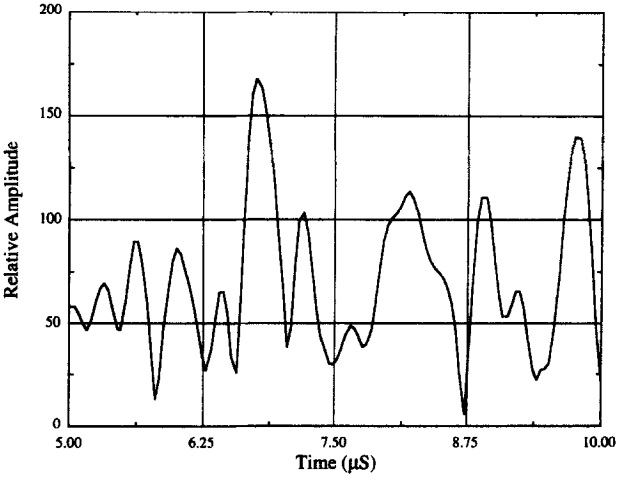

Fig. 10. Envelope of an RF A-line from the simulated data.

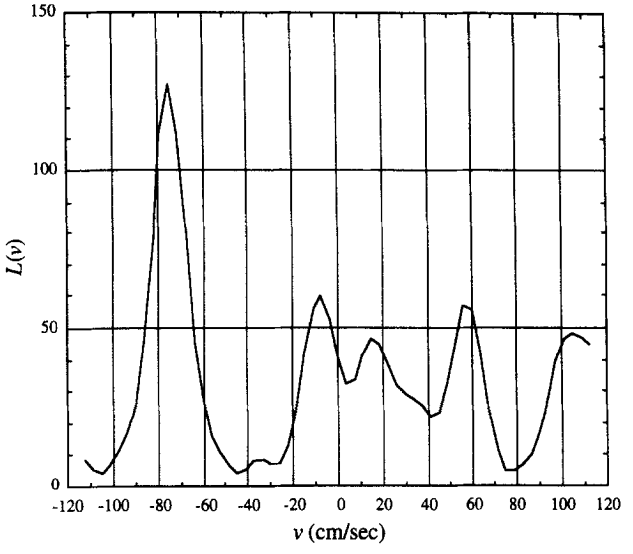

Fig. 11. $L(v)$ *vs.* v, for four RF lines. Actual velocity is −75 cm/s, no additive noise present. $L(v)$ maximizes at −75 cm/s.

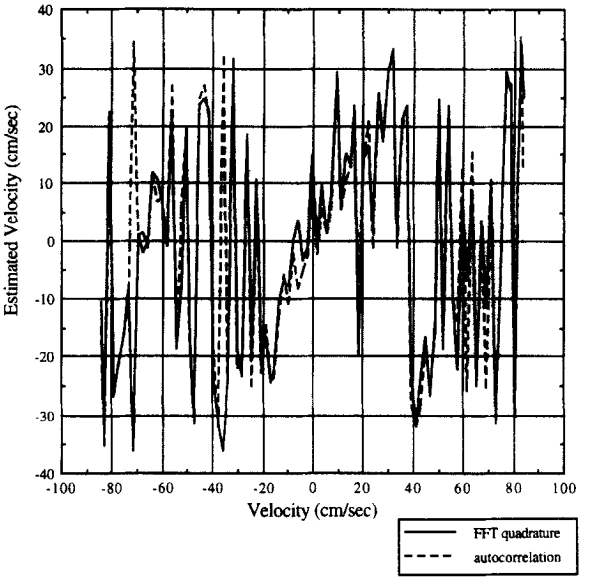

Fig. 13. Performance of FFT quadrature and autocorrelation method. Number of RF lines = 3, SNR = 0 dB.

The performances of different estimation techniques on the simulated data for three RF lines are shown in Figs. 13 to 17. The SNR was 0 dB. These are very unfavorable conditions which test the robustness of each technique. The estimation is done only at one range. Each simulation used a constant velocity and the range of simulations was −83.75 cm/s to 83.75 cm/s. As expected, both quadrature FFT and autocorrelation (Fig. 13) methods suffer from aliasing problem, which limits their range of accurate velocity estimation. However, neither method was very accurate even within the nonaliasing interval (−37.5 to 37.5 cm/s).

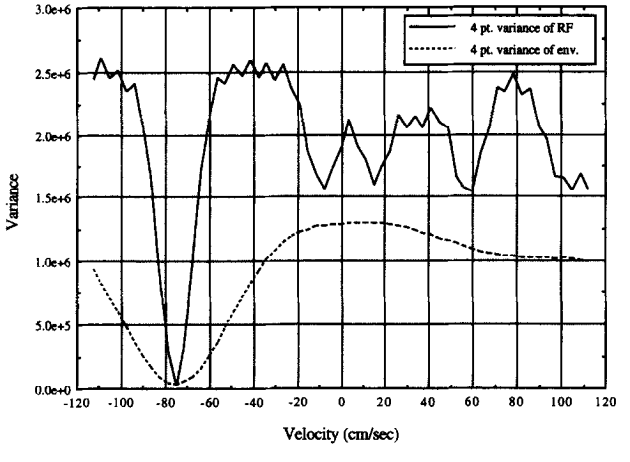

Fig. 12. Variance of RF (solid line) and envelope (dashed line) on the butterfly lines corresponding to velocity v. Number of RF lines = 4. Actual velocity is −75 cm/s, with no additive noise present. Variance minimizes at −75 cm/s.

With the same conditions, the correlation and the SAD (Fig. 14) methods on RF signals perform similarly. One obvious advantage was that neither technique suffer from aliasing.

The butterfly search on RF (Fig. 15) did a fairly accurate estimation over the entire range of investigation. Butterfly search on quadrature components (Fig. 16) works well compared to other techniques and, it outperforms the butterfly search on RF slightly. The butterfly search on envelope (Fig. 17) did not perform well. Note that none of the butterfly techniques suffer from aliasing.

PHANTOM EXPERIMENTS AND RESULTS

Estimation results from an experiment involving progressively moving a phantom is given in this section. In the experiment, the phantom is repeatedly moved in a computer-controlled set-up between data acquisitions by a fixed amount to simulate velocity. In such an experiment, no velocity profile would be present. But, it is possible to generate precise motion in such a set-up. The experiment was done first with no transverse motion. Afterwards, off-axis motion was introduced to observe its effect on the estimation. A panametrics transducer was used for the scanning. The center frequency was 4 MHz and the sampling frequency was 40 MHz. The data were quantized at ten bits. A total of 2048 sample points were collected for every transducer firing. The beam width at the depth of consideration was ~1 mm. The pulse duration was 1 μs (PRF = 5 KHz). The phantom used was a tissue mimicking material from ATS labs (Norwalk, CT).

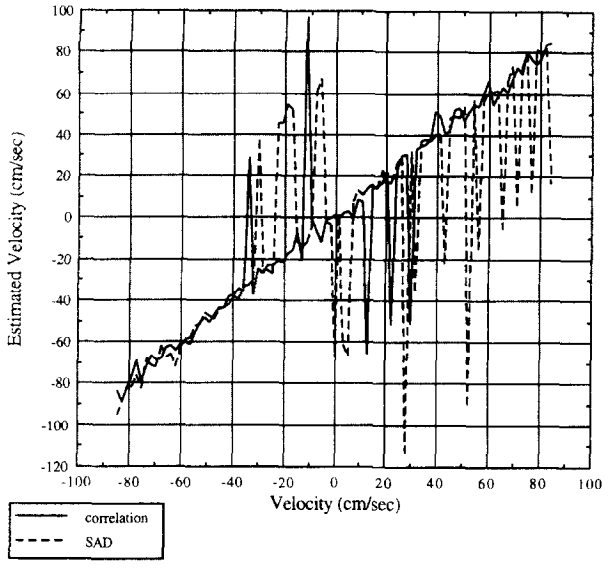

Fig. 14. Performance of correlation and SAD search techniques applied on RF. Number of RF A-lines = 3, SNR = 0 dB.

Fig. 18 shows the performance comparison of butterfly search on quadrature components, butterfly search on RF signal and RF cross-correlation with no transverse motion present. The number of RF A-lines used in the estimation was three. The butterfly search on quadrature components produced the most accurate estimates, followed in terms of accuracy by the butterfly search on RF signal and RF cross-correlation. The estimations were done at a depth of 2.85 cm. The SNR was calculated to be ~1.65 dB at this depth. A butterfly search on quadrature components was found to work well, even in the presence of such strong noise.

Fig. 19 shows the effect of off-axis movement on

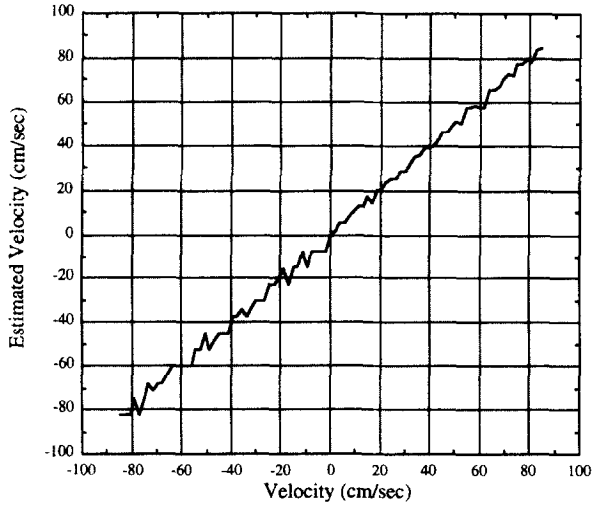

Fig. 15. Performance of butterfly search on RF. Number of RF lines = 3, SNR = 0 dB.

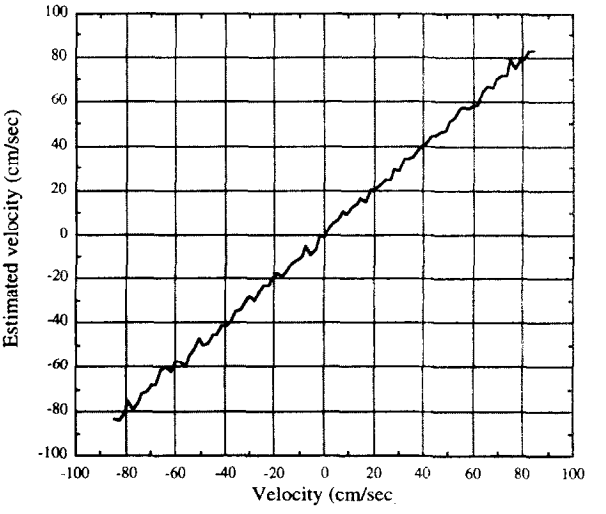

Fig. 16. Performance of butterfly search on quadrature components. Number of RF lines = 3, SNR = 0 dB.

the axial velocity estimation. The actual simulated axial velocity was −25 cm/s and three RF A-lines had been used. The estimations were done at a depth of 1.5 cm. The SNR was calculated to be ~25 dB at this depth. So, the estimation errors can primarily be attributed to transverse motion. The plot shows percent error magnitude *vs.* off-axis velocity. The error magnitudes were averaged over 14 cases. Complete speckle decorrelation, caused by large transverse motion, occurred around an off-axis velocity component of 750 cm/s. Both butterfly search on quadrature components and RF correlation search perform acceptably well below this velocity. Once speckles are completely decorrelated, the estimation algorithms fail and the value of the error is random. The autocorrelation technique had

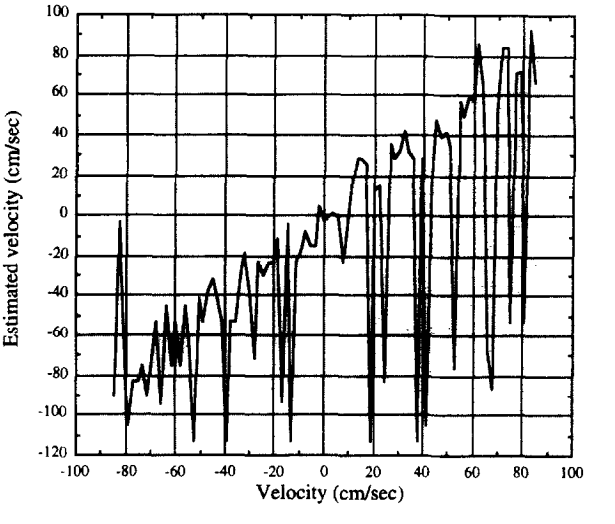

Fig. 17. Performance of butterfly search on envelope. Number of RF lines = 3, SNR = 0 dB.

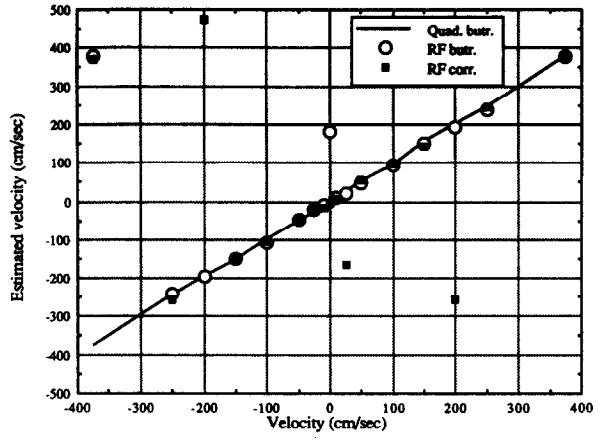

Fig. 18. Performance of different techniques in phantom experiment.

larger error than the other two before decorrelation occurred. However, this did not have the wild errors at higher off-axis velocities. The autocorrelation estimator, unlike the other two, produces estimates within the nonaliasing interval only. Within the range where complete speckle decorrelation has not occurred, there is a trend of the estimates to deviate more as the off-axis velocity increases.

For the estimations using both simulated data and phantom data, the data window for cross-correlation was about six wavelengths. To make the comparison meaningful, spatial averaging over six wavelengths was done on all techniques, which was equivalent to about 1 mm of tissue. Spatial averaging improved the performance because the additive noise was uncorrelated.

DISCUSSION AND CONCLUSIONS

A novel "butterfly search" technique for velocity estimation has been proposed. This technique has excellent noise and aliasing immunity, and is easily implemented in hardware with elementary digital operations. It does not suffer like the frequency domain methods with wider bandwidth pulses. So, there is no need for "toneburst" Doppler transmission. The performance graphs presented provide evidence that the butterfly search on quadrature components improves the accuracy of velocity estimation in high noise environments with few samples. The fact that it can perform so well even with only three RF A-lines (which would improve the frame rate of color Doppler imaging) in the presence of significant noise (SNR ~0 dB) is promising. However, the results shown are from just one realization of noise with moving scatterers. A more complete statistical analysis of competing estimators (with both simulations, and experimental results) over an ensemble of echoes is the subject of further investigation.

Although our approaches to the butterfly search have been derived from a deterministic analysis of the signals along a target trajectory, it should be noted that the butterfly search can be related to other conceptual starting points. An important example is the wideband MLE that was proposed and developed by Ferrara and Algazi (1991a,b). As discussed in the background section, eqn (8) for the WMLE is derived from a framework that is consistent with the classical matched filter. However, under a number of specific assumptions and modifications, eqn (8) could be modified into the form of the butterfly search on quadrature components, as described in eqn (20). A number of key modifications need to be made, including: (1) the matched filter should be changed to a rectangular window; (2) the continuous complex exponential term is changed to a discrete form; (3) the higher order term involving v is dropped from the argument of the complex exponential; (4) a denominator normalization term is included. These are shown in Appendix II.

Another conceptual framework that could be related logically to the butterfly search is the discrete Radon transform which has some uses in beamforming (Johnson and Dudgeon 1993). Our butterfly search could be considered a search for the maximum output value along lines of constant "intercept" of a Radon transform, in analogy to the envelope and RF butterfly search examples of Figs. 4 and 5. Also, see Durrani and Bisset (1984) for an overview of Radon transform and its properties.

The Radon transform is also known as the $\tau-p$ transform, and is used for seismic data analysis by the geophysicists. It is known that the delay-time (τ-p) parameterization of seismic travel-time data has sev-

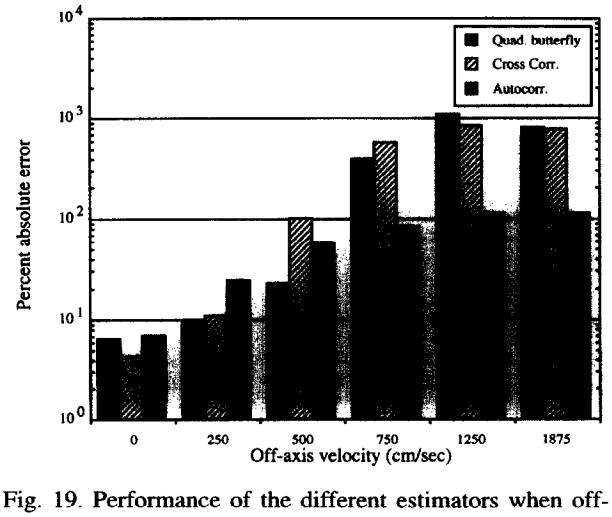

Fig. 19. Performance of the different estimators when off-axis component is present. Number of lines = 3.

eral advantages over the time-distance (T-X) representation. Many $\tau-p$ transform methods are available for seismic data analysis. For a comparison, see Kappus et al. (1990).

Each conceptual framework, our deterministic analysis of trajectory, the matched filter estimator and the discrete Radon transformer, gives a unique insight into the problem of estimating target velocity, and the contribution of this study is in the novel description of the problem; the form of unified estimators for envelope, RF, and complex signals; and the novel hardware implementation which is conducive to parallel and real-time processing for color imaging systems.

Acknowledgements—This work was supported in part by the Department of Electrical Engineering and the NSF/NYS Center for Electronic Imaging System. We would also like to thank Prof. Tekalp of Electrical Engineering, University of Rochester, for valuable discussions regarding simulations, and Dr. Xucai Chen of Electrical Engineering, University of Rochester, for the help in collecting the phantom data. We are grateful to Dr. Kathy Ferrara for helpful discussions concerning WMLE. We also thank the anonymous reviewers for their valuable comments.

REFERENCES

Angelsen, B. A. J. Instantaneous frequency, mean frequency, and variance of mean frequency estimators for ultrasonic blood velocity Doppler signals. IEEE Trans. Biomed. Eng. BME-28:733–741; 1981.

Baek, K. R.; Bae, M. H.; Park, S. B. A new aliasing extension method for ultrasonic 2-dimensional pulsed Doppler systems. Ultrason. Imaging 11:233–244; 1989.

Barber, W. D.; Eberhard, J. W.; Karr, S. G. A new time domain technique for velocity measurements using Doppler ultrasound. IEEE Trans. Biomed. Eng. BME-32:213–229; 1985.

Bohs, L. N.; Trahey, G. E. A novel method for angle independent ultrasonic imaging of blood flow and tissue motion. IEEE Trans. Biomed. Eng. BME-38:280–286; 1991.

Bonnefous, O.; Pesque, P. Time domain formulation of pulse-Doppler ultrasound and blood velocity estimation by cross correlation. Ultrason. Imaging 8:73–85; 1986.

Bracewell, R. N. The Fourier transform and its applications. New York: McGraw-Hill; 1986.

Durrani, T. S.; Bisset, D. The Radon transform and its properties. Geophysics 49:1180–1187; 1984.

Embree, P. M.; O'Brien, W. D., Jr. Volumetric blood flow via time-domain correlation: experimental verification. IEEE Trans. Ultrason. Ferroelec. Freq. Contr. 37:176–189; 1990.

Fan, L.; Evans, D. H. Extracting instantaneous mean frequency information from Doppler signals using the Wigner distribution function. Ultrasound Med. Biol. 20:429–443; 1994.

Ferrara, K. W.; Algazi, V. R. A new wideband spread target maximum likelihood estimator for blood velocity estimation—part I: Theory. IEEE Trans. Ultrason. Ferroelec. Freq. Contr. 38:1–16; 1991a.

Ferrara, K. W.; Algazi, V. R. A new wideband spread target maximum likelihood estimator for blood velocity estimation—Part II: Evaluation of estimators with experimental data. IEEE Trans. Ultrason., Ferroelec. Freq. Contr. 38:17–26; 1991b.

Foster, S. G.; Embree, P. M.; O'Brien, W. D., Jr. Flow velocity profile via time-domain correlation: Error analysis and computer simulation. IEEE Trans. Ultrason., Ferroelec. Freq. Contr. 37:164–175; 1990.

Hein, I. A.; O'Brien, W. D., Jr. Current time-domain methods for assessing tissue motion by analysis from reflected ultrasound echoes—a review. IEEE Trans. Ultrason. Ferroelec. Freq. Contr. 40:84–102; 1993.

Helstorm, C. W. Statistical theory of signal detection. New York: Pergamon Press; 1960.

de Jong, P. G. M.; Arts, T.; Hoeks, A. P. G.; Reneman, R. S. Determination of tissue motion velocity by correlation interpolation of pulsed ultrasonic signals. Ultrason. Imag. 12:84–98; 1990.

Johnson, D. H.; Dudgeon, D. E. Array signal processing: concepts and techniques. Englewood Cliffs, NJ: Prentice-Hall; 1993.

Kappus, M. E.; Harding, A. J.; Orcutt, J. A. A comparison of tau-p transform methods. Geophysics 55:1202–1215; 1990.

Kasai, C.; Namekawa, K.; Koyano, A.; Omoto, R. Real-time two-dimensional blood flow imaging using an autocorrelation technique. IEEE Trans. Son. Ultrason. SU-32:458–464; 1985.

Magnin, P. A. Doppler effect: History and theory. Hewlett-Packard J. 37:26–31; 1986.

Mo, L. Y. L.; Yun, L. C. M.; Cobbold, R. S. C. Comparison of four digital maximum frequency estimators for Doppler ultrasound. Ultrasound Med. Biol. 14:355–363; 1988.

Oppenheim, A. V.; Willsky, A. S.; Young, I. T. Signals and systems. Englewood Cliffs, NJ: Prentice-Hall; 1983.

Pesque, P. R. A. Apparatus for examining a moving object by means of ultrasound echography. United States Patent No. 4,853,904; Aug. 1989.

Sturgill, M. R.; Love, R. H.; Herres, B. K. An improved blood velocity estimator optimized for real-time ultrasound flow applications. IEEE 1990 Ultrasonics Symposium Proceedings; 1467–1471.

Vaitkus, P. J.; Cobbold, R. S. C. A comparative study and assessment of Doppler ultrasound spectral estimation techniques. Part I: Estimation methods. Ultrasound Med. Biol. 14:661–672; 1988.

Vaitkus, P. J.; Cobbold, R. S. C.; Johnston, K. W. A comparative study and assessment of Doppler ultrasound spectral estimation techniques. Part II: Methods and results. Ultrasound Med. Biol. 14:673–687; 1988.

Wilson, L. S. Description of broad-band pulsed Doppler ultrasound processing using the two-dimensional Fourier transform. Ultrason. Imaging 13:301–315; 1991.

APPENDIX I

Derivation of $L(v)$, *and proof that it maximizes only at* $v = v_0$:

Schwartz's inequality (Helstorm 1960) can be used to show that $L(v)$ maximizes at $v = v_0$. For continuous complex functions $g_1(t)$ and $g_2(t)$,

$$\text{if } \int_a^b |g_1(t)|^2 dt < \infty \quad \text{and} \quad \int_a^b |g_2(t)|^2 dt < \infty, \quad \text{(A.1.01a)}$$

$$\text{then } \left|\int_a^b g_1(t)g_2(t)dt\right|^2 \le \int_a^b |g_1(t)|^2 dt \int_a^b |g_2(t)|^2 dt. \quad \text{(A.1.01b)}$$

The equality is satisfied only when

$$g_1(t) = kg_2(t) \quad \text{(A.1.01c)}$$

where k is a constant.

In its discrete form the inequality can be expressed as follows. If

$$\sum_n |g_1[n]|^2 < \infty \quad \text{and} \quad \sum_n |g_2[n]|^2 < \infty, \quad \text{(A.1.02a)}$$

then

$$\left|\sum_n g_1[n]g_2[n]\right|^2 \leq \sum_n |g_1[n]|^2 \sum_n |g_2[n]|^2. \quad \text{(A.1.02b)}$$

The equality is satisfied only when

$$g_1[n] = kg_2[n]. \quad \text{(A.1.02c)}$$

With reference to eqns (18) and (20), let us define

$$g_1[n] = \tilde{A} \exp j\left\{2\omega_0 n \frac{v - v_0}{c} T\right\} \quad \text{and}$$

$$g_2[n] = r\left(2n \frac{v_0 - v}{c} T\right). \quad \text{(A.1.03)}$$

Then,

$$\left|\sum_{n=0}^{N_0} \tilde{A} \exp j\left\{2\omega_0 n \frac{v - v_0}{c} T\right\} r\left(2n \frac{v_0 - v}{c} T\right)\right|^2$$

$$\leq \sum_{n=0}^{N_0} \left|\tilde{A} \exp j\left\{2\omega_0 n \frac{v - v_0}{c} T\right\}\right|^2 \sum_{n=0}^{N_0} \left|r\left(2n \frac{v_0 - v}{c} T\right)\right|^2. \quad \text{(A.1.04)}$$

If there are $N_0 + 1$ terms in the summations, the first sum on the right side of the inequality equals $(N_0 + 1)|\tilde{A}|^2$.

Thus

$$\frac{\left|\sum_n \tilde{A} \exp j\left\{2\omega_0 n \frac{v - v_0}{c} T\right\} r\left(2n \frac{v_0 - v}{c} T\right)\right|^2}{\sum_n \left|r\left(2n \frac{v_0 - v}{c} T\right)\right|^2} \leq (N_0 + 1)|\tilde{A}|^2 \quad \text{(A.1.05)}$$

Or

$$\frac{\left|\sum_n \tilde{A} \exp -j\left\{2\omega_0 n \frac{v_0}{c} T\right\} r\left(2n \frac{v_0 - v}{c} T\right) \exp j\left\{2\omega_0 n \frac{v}{c} T\right\}\right|^2}{\sum_n \left|\tilde{A} \exp -j\left\{2\omega_0 n \frac{v_0}{c} T\right\} r\left(2n \frac{v_0 - v}{c} T\right)\right|^2} \leq (N_0 + 1), \quad \text{(A.1.06)}$$

Since

$$\left|\exp -j\left\{2\omega_0 n \frac{v_0}{c} T\right\}\right| = 1. \quad \text{(A.1.07)}$$

Or

$$\frac{\left|\sum_n \tilde{r}_{Bv}[n] e^{j2\omega_0 n(v/c)T}\right|^2}{\sum_n |\tilde{r}_{Bv}[n]|^2} \leq (N_0 + 1), \quad \text{(A.1.08)}$$

Since

$$\tilde{r}_{Bv}[n] = \tilde{A} \exp -j\left\{2\omega_0 n \frac{v_0}{c} T\right\} r\left(2n \frac{v_0 - v}{c} T\right). \quad \text{(A.1.09)}$$

Or

$$L(v) \leq (N_0 + 1). \quad \text{(A.1.10)}$$

Both $g_1[n]$ and $g_2[n]$ become constants at $v = v_0$. Thus, the condition $\frac{g_1[n]}{g_2[n]} = k$ is satisfied only at $v = v_0$. And, thus $L(v) \leq L(v_0)$, and the maximum is only at $v = v_0$.

APPENDIX II

Relating the concepts of the butterfly search on quadrature components to the WMLE

The wideband maximum likelihood estimator developed by Ferrara and Algazi (1991a,b) is given by

$$l(v) = \left|\sum_k \int_{-\infty}^{\infty} r'(t)s'^*\left(t - \tau_0 - kT\left[1 + 2\frac{v}{c}\right]\right) \exp\left(j2\omega_0 \frac{v}{c} t\right) dt\right|^2. \quad \text{(A.2.01)}$$

Now assume that a rectangular window of size w is used instead of the matching signal $s'^*(\cdot)$, then

$$l(v) \approx \left|\sum_k \int_{\tau_0 + kT[1 + 2(v/c)] - (w/2)}^{\tau_0 + kT[1 + 2(v/c)] + (w/2)} r'(t) e^{j2\omega_0 (v/c)t} dt\right|^2. \quad \text{(A.2.02)}$$

Next, we include the assumption, $f_0 \frac{v}{c} w \ll 1$, to convert the complex exponential inside the integral to a discrete exponential that remains constant within the integration interval. Then, we take it out of the integral

$$l(v) \approx \left|\sum_k e^{j2\omega_0 (v/c)kT[1 + 2(v/c)]} \int_{\tau_0 + kT[1 + 2(v/c)] - (w/2)}^{\tau_0 + kT[1 + 2(v/c)] + (w/2)} r'(t) dt\right|^2. \quad \text{(A.2.03)}$$

With a variable substitution

$$l(v) \approx \left|\sum_k e^{j2\omega_0 (v/c)kT[1 + 2(v/c)]} \times \int_{-w/2}^{w/2} r'\left[t - \tau_0 - kT\left(1 + 2\frac{v}{c}\right)\right] dt\right|^2. \quad \text{(A.2.04)}$$

Now, if this integral window is shrunk to a size small enough such that the integrand would remain nearly a constant within the window, and the integral can be replaced by the integrand multiplied by a constant factor w, we obtain

$$I(v) \approx \left| \sum_k e^{j2\omega_0(v/c)kT[1+2(v/c)]} wr'\left[t - \tau_0 - kT\left(1 + 2\frac{v}{c}\right)\right]\right|^2. \quad \text{(A.2.05)}$$

Next, we assume that v^2/c^2 can be neglected, then

$$I(v) \approx \left| \sum_k e^{j2\omega_0(v/c)kT} wr'\left[t - \tau_0 - kT\left(1 + 2\frac{v}{c}\right)\right]\right|^2. \quad \text{(A.2.06)}$$

If the time-axis origin is not reset after each firing, then our quadrature butterfly $L(v)$ will have the following form

$$L(v) = \frac{\left| \sum_n e^{j2\omega_0(v/c)nT} \tilde{r}\left[t - 2\frac{d}{c} - nT\left(1 - 2\frac{v}{c}\right)\right]\right|^2}{\left| \sum_n \tilde{r}\left[t - 2\frac{d}{c} - nT\left(1 - 2\frac{v}{c}\right)\right]\right|^2}. \quad \text{(A.2.07)}$$

Clearly, eqn (A.2.06) and (A.2.07) are similar except for the scale factor w, and a normalization factor has to be applied in eqn (A.2.06) to convert it to eqn (A.2.07) form. Thus, a relationship can be established between the modified form of WMLE and the butterfly search on quadrature component implementation. The reason for a difference in the sign before the $2v/c$ term has not been determined.